Geophysical Research Letters

RESEARCH LETTER
10.1029/2018GL081354

Warm Circumpolar Deep Water at the Western Getz Ice Shelf Front, Antarctica

K. M. Assmann[1], E. Darelius[2], A. K. Wåhlin[1], T. W. Kim[3], and S. H. Lee[3]

[1]Department of Marine Sciences, University of Gothenburg, Gothenburg, Sweden, [2]Geophysical Institute, University of Bergen and the Bjerknes Centre for Climate Research, Bergen, Norway, [3]Korea Polar Research Institute, Incheon, South Korea

Key Points:
- Observations show a persistent flow of warm (Theta > 0.5 degrees Celsius) Circumpolar Deep Water toward the western front of the Getz Ice Shelf
- Unmodified CDW reaches the ice shelf front episodically and is present there 7.5% of the time
- The depth of the thermocline is determined by zonal wind stress and upwelling at the shelf break

Supporting Information:
- Supporting Information S1
- Figure S1
- Figure S2

Correspondence to:
E. Darelius,
elin.darelius@uib.no

Citation:
Assmann, K. M., Darelius, E., Wåhlin, A. K., Kim, T. W., & Lee, S. H. (2019). Warm Circumpolar Deep Water at the western Getz Ice Shelf front, Antarctica. *Geophysical Research Letters*, *46*, 870–878. https://doi.org/10.1029/2018GL081354

Received 16 NOV 2018
Accepted 2 JAN 2019
Accepted article online 4 JAN 2019
Published online 30 JAN 2019

Abstract The Getz Ice Shelf is one of the largest sources of fresh water from ice shelf basal melt in Antarctica. We present new observations from three moorings west of Siple Island 2016–2018. All moorings show a persistent flow of modified Circumpolar Deep Water toward the western Getz Ice Shelf. Unmodified Circumpolar Deep Water with temperatures up to 1.5 °C reaches the ice shelf front in frequent episodes. These represent the warmest water observed at any ice shelf front in the Amundsen Sea. Mean currents within the warm bottom layer of 18–20 cm/s imply an advection time scale of 7 days from shelf break to ice shelf front. Zonal wind stress at the shelf break affects heat content at the ice shelf front on weekly to monthly time scales. Our 2-year mooring records also evince that upwelling over the shelf break controls thermocline depth on subannual to annual time scales.

Plain Language Summary The recent retreat of the West Antarctic Ice Sheet has been linked to changes in the transport of warm ocean water up to 1.5 °C to the floating ice shelves in the Amundsen Sea. One of these is the Getz Ice Shelf that produces one of the largest amounts of ice shelf melt water in Antarctica. To measure how much ocean heat is transported toward this ice shelf, we deployed a series of temperature, salinity, and current sensors at its western end from 2016 to 2018. We find a constant flow of warm water toward the ice shelf cavity. Comparing our ocean observations with wind data from the area, we found that stronger easterly winds in the area make it harder for the warm water to reach the ice shelf front by depressing the warm bottom layer over the shelf break. Climate projections indicate that these easterlies will weaken in future, making it easier for the warm water to reach the ice shelf base. Gradients in the wind field over the shelf break control the thickness of the warm layer on longer time scales. This provides the missing ocean evidence for previous studies that have linked this wind mechanism to ice sheet changes.

1. Introduction

With an area of 34,018 km^2 the Getz Ice Shelf (GIS) is the eighth largest ice shelf in Antarctica (Rignot et al., 2013). A mean basal melt rate of 4.3 m/year makes it one of the largest contributors of ice shelf basal meltwater (Depoorter et al., 2013; Rignot et al., 2013). Model results suggest that GIS meltwater travels west with the coastal current (Nakayama et al., 2014) and has likely contributed to the observed freshening in the dense Ross Sea shelf waters (Jacobs et al., 2002). Changes in GIS basal melting thus have potential implications for Antarctic Bottom Water formation in the Ross Sea. The GIS has received much less attention than Thwaites Ice Shelf and Pine Island Glacier further east in the Amundsen Sea due to their higher basal melt rates and larger ice sheet drainage basins. However, thinning rates for the GIS have accelerated over recent decades (Paolo et al., 2015) and its grounding line is retreating (Christie et al., 2018) raising questions about its future evolution and its impact on water mass formation processes, both locally and downstream in the Ross Sea.

The GIS extends for 650 km along the West Antarctic coast between 115°W and 135°W (Figure 1a). Its geometry is complex with multiple openings between six islands that serve as pinning points. It is unclear if there is a connection between the eastern and western parts of the cavity below the thickest part of the ice shelf (Figure 1a) as inferred by Jacobs et al. (2013) or what pathways allow the shelf water masses to access the grounding line.

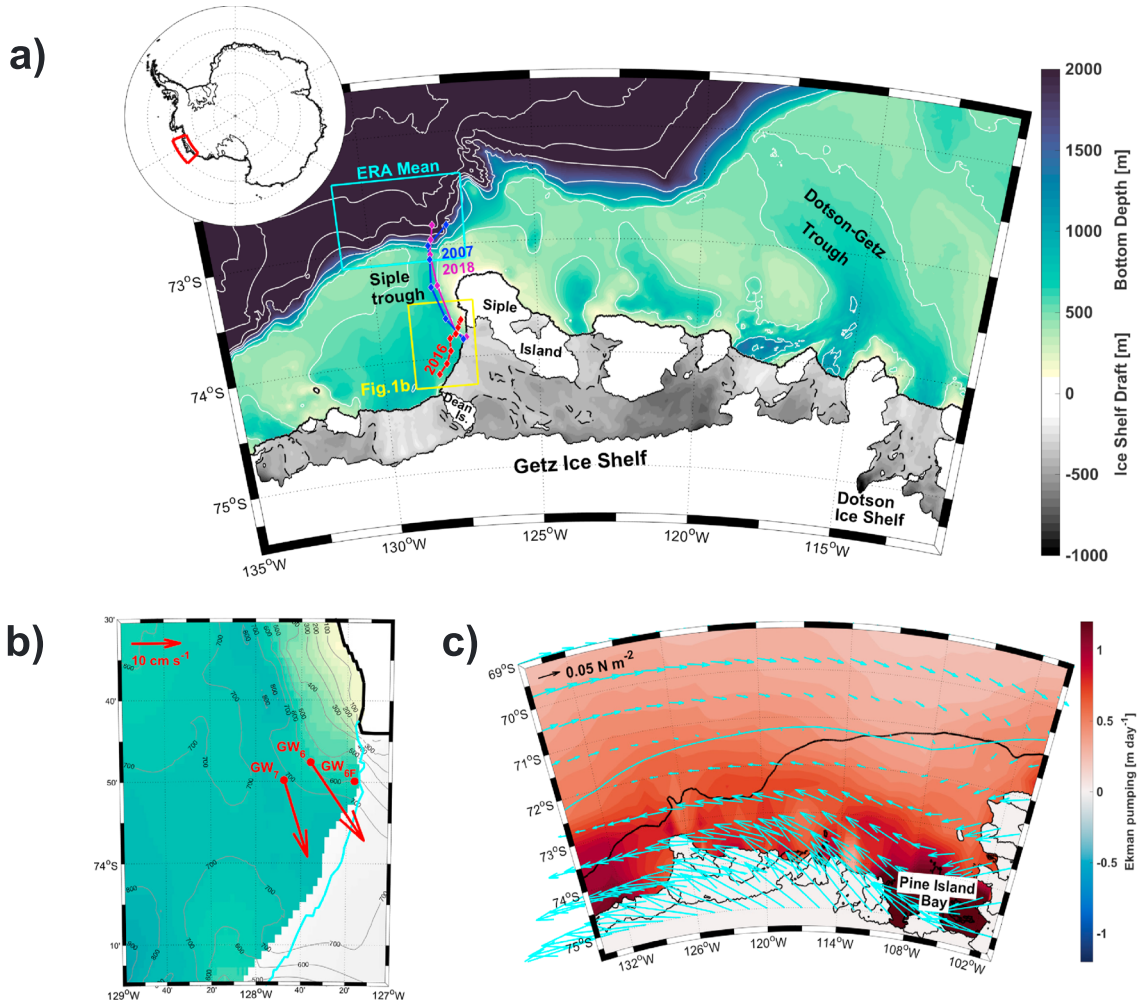

Figure 1. (a) Map of the Amundsen Sea. Bottom depth (colored, positive) and ice shelf draft (gray scale, negative) are from RTOPO2 (Schaffer et al., 2016). The yellow box marks the area shown in (b) and the cyan box the area over which wind stress, Ekman pumping, and sea ice concentration data were averaged. Blue, red, and purple lines and diamonds denote the sections shown in Figure 3. (b) Map of the inflow region to the western Getz Ice Shelf. Bottom depth is from IBCSO (Arndt et al., 2013) and the masked ice shelf front from RTOPO2 (Schaffer et al., 2016). The cyan line is the actual ice shelf edge in November 2015 from a satellite image (E. P. Abrahamsen, personal communication, 10 December 2015). The red arrows show the time-mean velocity for water with $\Theta > 0.0$ °C. (c) Map of the mean (November 2015 to January 2018) ERA-Interim wind stress (cyan vectors, every second zonal point is shown for clarity) and Ekman pumping velocity (colored shading). The mean position of the zero contour of the zonal wind stress is marked by the cyan line. The fat black line marks the 1,000-m isobath.

The hydrography in the basin adjacent to the eastern GIS and in the Dotson-Getz trough (Figure 1a) is relatively well observed. While moorings in the trough show persistent modified Circumpolar Deep Water (CDW) transport toward the Dotson and eastern Getz Ice Shelves (Arneborg et al., 2012; Wåhlin et al., 2013), the thermocline is deeper and modified CDW temperatures near the ice shelf fronts are lower than those found in Pine Island Bay (Jacobs et al., 2012; Randall-Goodwin et al., 2015). Dedicated oceanographic observations from the continental shelf adjacent to the western GIS front were until recently limited to two cruises in 2000 and 2007 with no records of temporal variability.

In this study, we present new observations from the trough cutting across the continental shelf in front of the main western opening of the GIS between Siple and Dean Island, hereafter referred to as the Siple trough (Figure 1a). We use temperature and velocity records from three moorings deployed on the eastern slope of the Siple trough 2016–2018 (Figure 1b) to show that there is a persistent flow of warm water toward the western GIS cavity through the Siple trough. We investigate the subannual variability of the warm water inflow and thermocline depth and identify possible driving mechanisms.

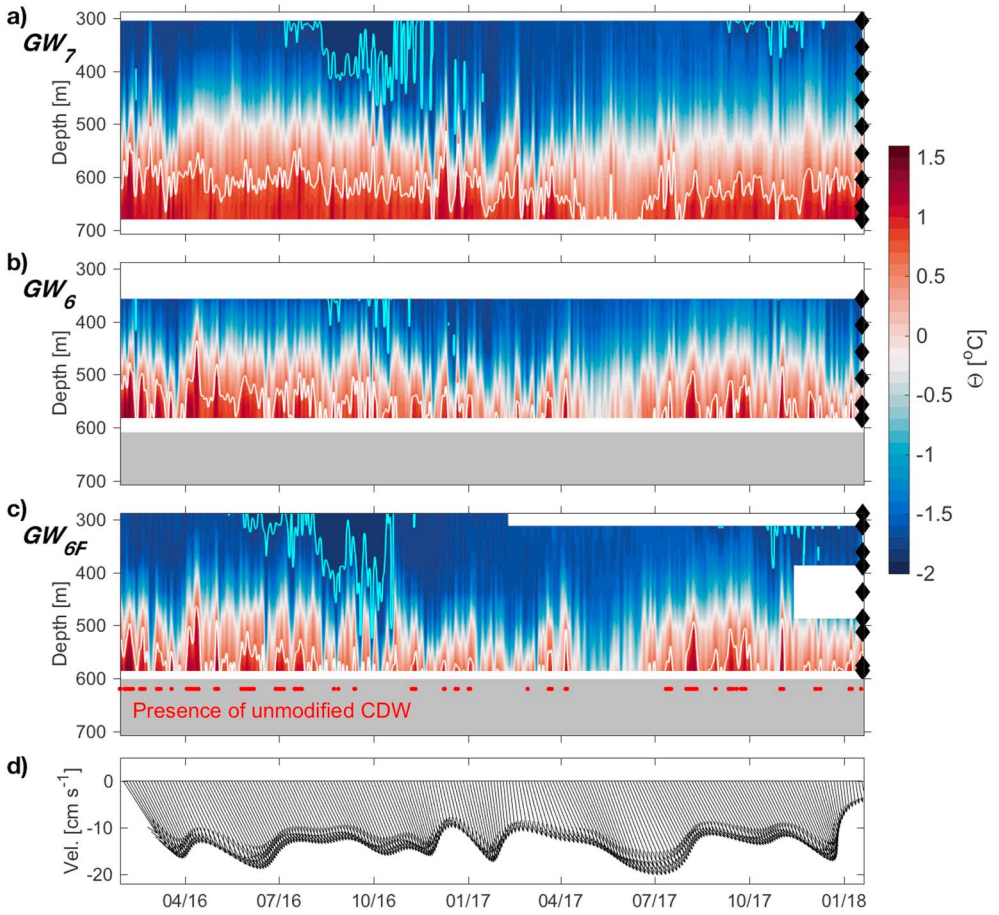

Figure 2. Hovmøller diagrams of 2-day low-pass filtered conservative temperature, Θ, versus time and depth for (a) GW_7, (b) GW_6, and (c) GW_{6F}. Contours marked are −1.8 °C (cyan) and 0.7 °C (white). Red dots in (c) mark the presence of unmodified CDW (Θ > 1 °C, S_A > 34.85 g/kg, green box in Figure 3c). Black diamonds indicate the position of the hydrographic sensors. The gray panels in (b) and (c) indicate the depth of the ocean floor. (d) Mean GW_6 velocity below 500-m depth. Shown are low-pass filtered 3-day means. The length of the arrows indicates flow speed and their direction its cardinal direction. CDW = Circumpolar Deep Water.

2. Data and Methods

Three moorings were deployed on the eastern flank of the Siple trough between 29 January 2016 and 18 January 2018 (Figure 1b). Two of the moorings were deployed 15 km from the ice shelf front at depths of 600 m (GW_6, 73°47.6′S, 127°36.0′S) and 700 m (GW_7, 73°49.8′S, 127°47.6′S). The third mooring was located around 800 m from the ice shelf front at a depth of 600 m (GW_{6F}, 73°50.0′S, 127°16.6′S). The moorings were equipped with sensors for temperature, conductivity, and pressure from Seabird Electronics (SBE37, SBE39, and SBE56) and Acoustic Doppler Current Profilers (Teledyne RDI, 75 and 150 kHz). Hydrographic measurements extended from the bottom to 357- and 305-m depth for GW_6 and GW_7, respectively, with downward looking Acoustic Doppler Current Profilers just above the top sensor, and to 288-m depth, approximately the same depth as the draft of the ice shelf front, at GW_{6F} (Figures 2a–2c).

In this study we present the data following TEOS-10 (IOC et al., 2010) as conservative temperature, Θ (°C), and absolute salinity, S_A (g/kg), where S_A is calculated using δS_A taken from version 3.6 of the McDougall et al. (2012) database. We define CDW as water with a neutral density γ_n larger than 28.0 kg/m^3 (Whitworth et al., 1998). Since some of the mooring instruments only measure temperature and not salinity, we use 0.7 °C as an equivalent criterium identified from a hydrographic section (Figure 3a) to indicate the presence of weakly modified CDW in the mooring records (Figures 2a–2c). To capture the temporal evolution of the thermocline, we computed the heat content with respect to the in situ freezing point.

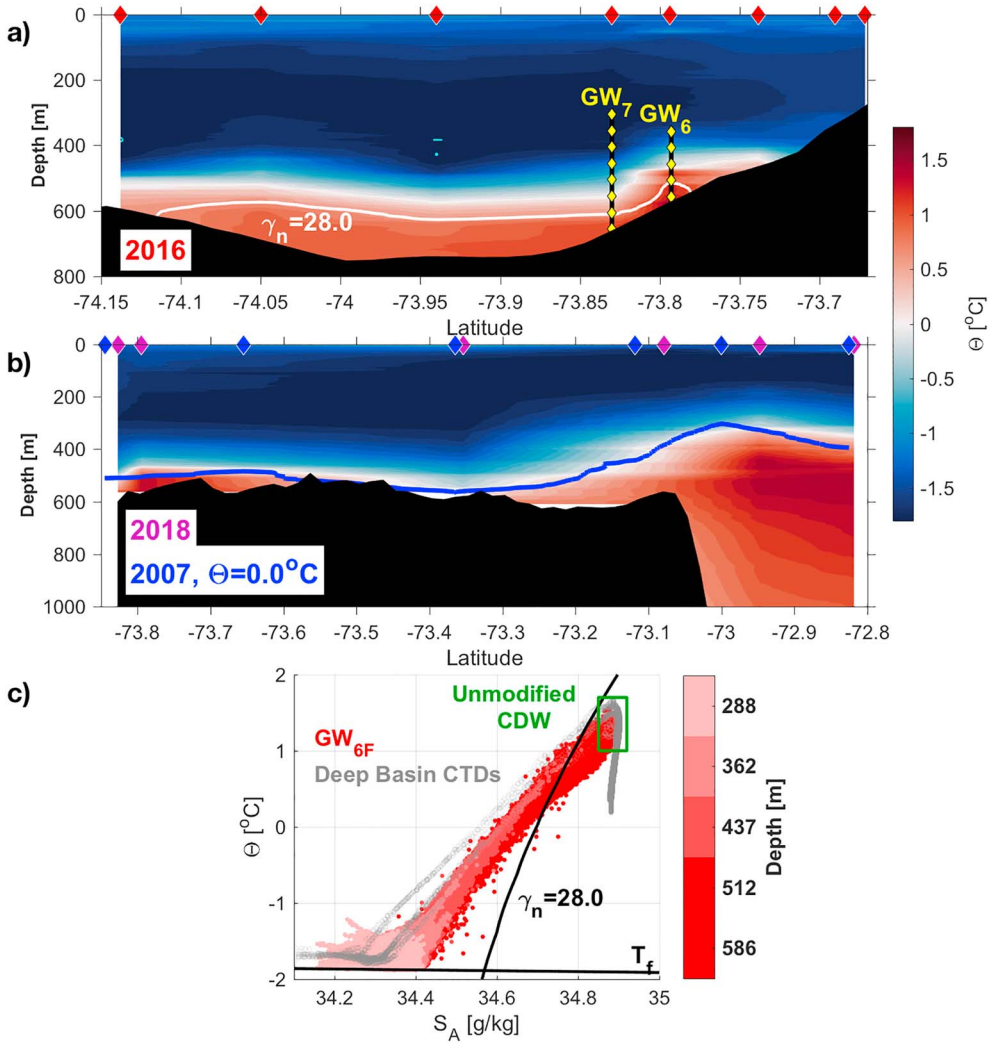

Figure 3. (a) The 2016 section of conservative temperature Θ along the western GIS front facing westward out of the ice shelf cavity. Station positions are marked as red diamonds in the section and in Figure 1a. The white contour is $\gamma_n = 28.0$ as the upper CDW limit. Also shown are the positions of GW_6 and GW_7 with the positions of the temperature sensors marked by yellow diamonds. (b) The 2018 Θ section across the shelf break with stations marked by purple diamonds at the top of the section and in Figure 1a. The $\Theta = 0.0$ °C isotherm is shown for a 2007 section (blue line and blue diamonds at the top and in Figure 1a). (c) Θ-S_A diagram for GW_{6F} (color coded by depth) and for historical CTD stations north of the Siple trough sill (light gray). The green box shows our definition for unmodified CDW ($\Theta > 1$ °C, $S_A > 34.85$ g/kg). GIS = Getz Ice Shelf; CDW = Circumpolar Deep Water.

To provide spatial and historical context for our mooring observations, we use ship-based hydrographic observations from the deployment and recovery cruises in 2016 (ANA06B) and 2018 (ANA08B) and historical CTD observations from 2000 and 2007. To investigate the driving mechanisms of the subannual temperature variability at the mooring sites, we used 12-hr mean turbulent surface stresses from the ERA-Interim Re-analyses (Dee et al., 2011) and high-resolution sea ice concentrations from AMSR2 (Spreen et al., 2008). All wind stress, Ekman pumping, and sea concentration time series in our analysis are averaged over the cyan box marked in Figure 1a at the shelf break.

3. Results

3.1. CDW Presence From Moorings

The three Siple trough moorings show a persistent warm bottom layer with mean temperatures of 0.92 ± 0.17 °C (GW_7), 0.66 ± 0.45 °C (GW_6), and 0.53 ± 0.52 °C (GW_{6F}) for the bottom instrument (Figures 2a–2c). Larger standard deviations for the two shallower moorings reflect that the thermocline is located closer

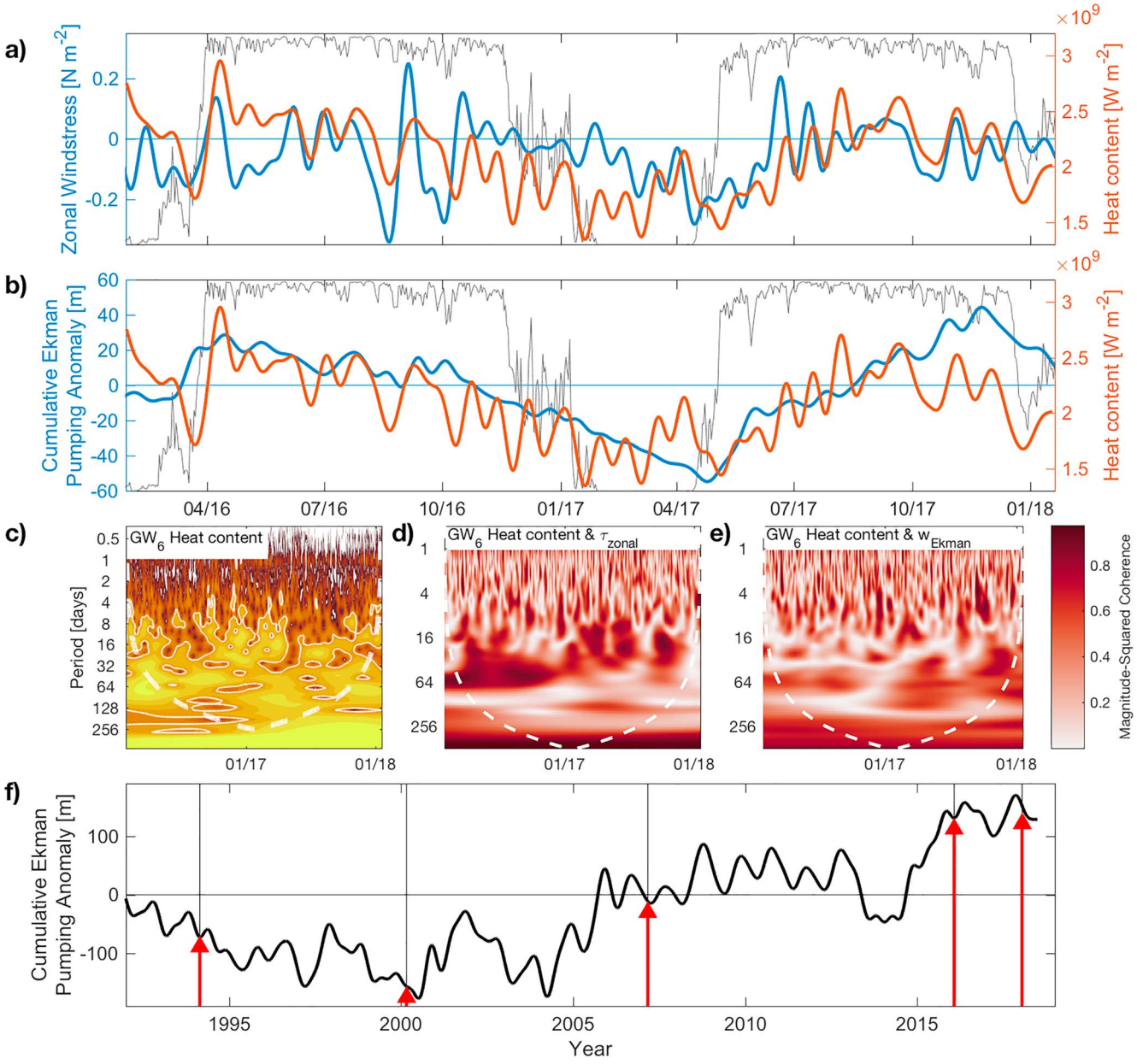

Figure 4. GW_6 heat content with respect to the in situ freezing point (red in a and b) together with (a) zonal wind stress (blue) and (b) the cumulative Ekman pumping anomaly (blue). All time series are 10-day low-pass filtered 12-hr means. Wind stress, Ekman pumping anomaly, and sea ice concentration (gray line in a and b) are averages over the cyan box in Figure 1a. (c) Wavelet analysis of the unfiltered, hourly GW_6 heat content showing how its frequency content changes over time. Yellow denotes higher power at a particular frequency at a given time. (d) Wavelet coherence between the GW_6 heat content and zonal wind stress at the shelf break. (e) Wavelet coherence between the 12-hr mean GW_6 heat content and the cumulative Ekman pumping anomaly at the shelf break. Darker red shading in (d) and (e) denotes high coherence between the two data sets at that frequency at a given time. The dashed white lines in (c), (d), and (e) show the cone of influence. End effects are expected below this line. (f) The 30-day low-pass filtered time series (1992–2018) of the cumulative Ekman pumping anomaly at the shelf break. Red arrows mark the cruise dates for the area.

to the bottom at these locations. The flow of water warmer than 0 °C is strong and persistent at the two moorings 15 km from the ice shelf edge (Figure 1b). It is directed along bathymetric contours toward the ice shelf front with mean flow speeds of 20 ± 2 cm/s and 18 ± 3 cm/s for GW_6 and GW_7, respectively. Bottom layer flow at GW_6 is persistently unidirectional over the mooring deployment with modulations in flow speed (Figure 2d).

A hydrographic section in January 2016 shows that a layer of warm CDW extends along the ice shelf front from Siple to Dean Island (Figure 3a). The warmest water is found at the northern end of the section as a core

centered at the 600-m isobath with a maximum conservative temperature of 1.59 °C. A similar section taken in January 2018 confirms the presence of this warm core (Figure S1 in the supporting information). Moorings GW_6 and GW_{6F} show that the presence of the weakly modified CDW seen in the sections is episodic (Figures 2b and 2c). Bottom temperatures at GW_6 and GW_{6F} are highly correlated with $r = 0.81$ for 2-day low-pass filtered temperatures. Apart from a period in May/June 2017, there is a persistent presence of CDW at mooring GW_7 where the basin is filled with water warmer than 0.7 °C below 600 m. The correlation for the bottom temperature of both GW_{6F} and GW_6 and the 600-m temperature at GW_7 is weaker at $r = 0.52$ for 2-day low-pass filtered data, presumably because GW_7 is within the pool of warm water that accumulates below the shelf break sill level of 590 m in the Siple trough.

CTD data obtained north of the western Getz shelf break have a CDW temperature maximum of 1.65 °C (Figure 3c). Comparing these stations to the GW_{6F} mooring observations in a Θ-S_A diagram reveals that there are episodes when the warm bottom layer reaches the ice shelf front unmodified without any significant cooling or freshening. Unmodified CDW ($\Theta > 1$ °C, $S_A > 34.85$ g/kg, green box in Figure 3c) is found at the bottom sensor on GW_{6F} for 7.5% of the mooring record in events that last between a few hours and up to a week (Figure 2c).

While there is obvious temperature variability on monthly time scales in our 2-year mooring records, they do not show any clear seasonality in the CDW layer temperature or thickness. They capture, however, the deepening of the freshly ventilated WW layer in late winter (Figures 2a–2c). Heat content variability in the mooring records is dominated by variability at time scales from 10 days to 2–3 months, that is, longer than time scales usually associated with synoptic variability (Figure 4c for GW_6). Variability on synoptic time scales only gains importance in the summer months when the sea ice cover recedes from the area (Figure 4a).

3.2. Atmospheric Forcing and Mechanisms Controlling CDW Inflow

The episodic presence of unmodified CDW at our moorings and the proximity of the shelf break suggests that shelf break processes may control CDW transport to the ice shelf front. Hydrographic sections from 2018 and 2007 show that there is a clear Antarctic Slope Front (ASF) at the shelf break north of the Siple trough with isopycnals sloping down 200 m across the shelf break (Figure 3b). None of the available CTD stations on the outer shelf reach the temperatures seen in the inflow near the ice shelf front. However, the presence of unmodified CDW at the ice shelf front in both mooring records and CTD sections implies that there must be episodes when the ASF weakens sufficiently to allow unmodified CDW onto the shelf. Since there are no mooring time series on the outer shelf, we will use the ERA-Interim data to infer possible control mechanisms.

The strength of the winds along the shelf break has been identified as a control of the structure of the ASF (Stewart & Thompson, 2015) with stronger easterlies depressing the thermocline more strongly across the shelf break and suppressing CDW access to the shelf. The average wind stress at the western Getz shelf break is zonal and easterly (Figure 1c) with a mean of -0.05 N/m^2. In addition, Ekman pumping has been invoked as a mechanism controlling thermocline depth in the inflow to the eastern GIS (Kim et al., 2017). To assess whether this effect can also be seen in the Siple trough, we calculated the accumulated Ekman pumping velocities over the shelf break (Figure 1a, cyan box) and detrended them to obtain a cumulative anomaly in meters from the mean upwelling rate of 0.85 m/day.

The cool period in summer and autumn 2017 (Figures 2a–2c) coincides with consistent, strong easterly wind stress (Figure 4a) and a negative anomaly in the cumulative Ekman pumping at the shelf break (Figure 4b). Zonal wind stress at the shelf break and GW_6 heat content have consistent coherence for periods between 10 and 64 days (Figure 4d). Individual peaks in the 10-day low-pass filtered time series can be matched easily, in particular two events of strong easterlies in September and October 2016 that are followed by a decrease in heat content at GW_6 with a lag of 4–8 days. The 10-day low-pass filtered GW_6 heat content and the zonal wind stress at the shelf break are correlated at $r = 0.42$, significant at the 99.9% level, with a 5-day lag. The cumulative Ekman pumping anomaly is dominated by 1- to 2-year variability (Figure 4e). The correlation between the cumulative Ekman pumping anomaly and the GW_6 heat content increases with increasing low-pass filtering limits yielding $r = 0.74$, significant at the 99% level, for 40-day low-pass filtered time series.

4. Discussion and Conclusions

Our moorings show a persistent inflow of warm CDW toward the western GIS cavity along the eastern flank of the Siple trough. Mean bottom temperatures are $\Theta = 0.5$–0.9 °C, but CDW reaches the ice shelf front essentially unmodified ($\Theta > 1.0$ °C) in regular hourlong to weeklong events. Maximum temperatures observed at the ice shelf front are only 0.1 °C lower than the CDW maximum temperature north of the shelf break (Figure 3c). Mean along-trough velocities of 20 cm/s for the two outer moorings imply an advection time scale of only 7 days to cross the 110-km distance between shelf break and ice shelf front.

Maximum CDW temperatures at the western GIS are around 0.6 °C higher than in Pine Island Bay that is filled with almost isothermal water with $\Theta = 0.8$–1.2 °C below 700 m (Dutrieux et al., 2014). While the ASF is much weaker at the two Pine Island Bay inflow troughs allowing continuous CDW access onto the shelf (Assmann et al., 2013), transport pathways across the 550-km-wide shelf to the ice shelf front are less direct than for the western GIS. This results in considerable cooling of the CDW across the shelf and highlights the uniqueness of the immediate connection between deep ocean and ice shelf cavity at the western GIS.

There is an inflow of warm CDW also toward the eastern GIS (Arneborg et al., 2012; Wåhlin et al., 2013). Offshore temperatures north of the Dotson-Getz Trough and the Siple trough are similar at $\Theta = 1.6$ °C, but mooring results and CTD stations in the Dotson-Getz Trough show that maximum temperatures in the inflowing CDW are about 0.6 °C lower than the off-shelf maximum (Wåhlin et al., 2013). This may be due to the shallower sill depth (510 m) and to the recirculation of glacial melt water in the Dotson-Getz Trough (Wåhlin et al., 2013). Weakly modified or unmodified CDW thus does not have access to the GIS cavity from the east.

Thermocline depth at the western GIS varies between 450 and 550 m in our mooring records. Variability of the CDW heat content is dominated by time scales of 10 days and longer. While our 2-year mooring records suggest that there is annual to interannual variability of the thermocline depth, there is no clear seasonal cycle in the thickness or temperature of the CDW layer. There is, however, evidence of deep ventilation of the water column in winter that in some years, like 2016, may be deep enough to reach the CDW layer.

Its more southern position places the shelf break sill of the Siple trough further into the band of easterly winds than the sills of the troughs further east in the Amundsen Sea. This leads to a clearly pronounced ASF (Figure 3b; see also Jacobs et al., 2012). Strong easterlies at the shelf break coincide with a cooler and thinner CDW layer at the ice shelf front, as they strengthen the ASF. This relationship is most coherent for periods from a week to a few months. There is a lag of 5–6 days between shelf break winds and heat content at the ice shelf front, possibly due to the advective time scale between the shelf break and the ice shelf front.

Anomalies in Ekman pumping at the shelf break are correlated to the heat content on longer time scales and explain 50% of the heat content variance. Kim et al. (2017) find a similar strength of correlation for bottom temperatures in the Dotson-Getz Trough and Ekman pumping velocities calculated from an ocean surface stress that includes the effect of sea ice. This suggests that the presence of sea ice does not strongly affect Ekman puming velocities over the Siple trough. The analysis by Kim et al. (2017) also shows strong coherence between Ekman pumping and CDW temperature and layer thickness at subannual time scales. In the Siple trough, the magnitude of the cumulative Ekman pumping anomaly is 100 m over the mooring period which is about the same scale of magnitude as the variability in thermocline depth that we see in our moorings. This strong link between Ekman pumping and mooring heat content at the ice shelf front provides some of the missing ocean data evidence in studies that have linked interannual changes in upwelling from wind stress curl to variability in ice flow velocities (Greene et al., 2017) and ice surface height (Paolo et al., 2018). It is likely that local downwelling along the Siple coast and the ice shelf front contributes to the observed variability in the heat content.

The circulation pattern in the intricate Getz cavity is unknown, but satellite-based melt rate patterns suggest that the weakly modified CDW with average temperature 3–4 °C above the in situ freezing point observed at our moorings may reach the deep grounding lines and induce strong melting there. Satellite-based basal melt rates exceed 5 m/year for these areas (Rignot et al., 2013), while Paolo et al. (2018) demonstrate that basal melt rates in these areas are highly sensitive to interannual changes in atmospheric circulation. Lower melt rates in the outer western GIS cavity (Rignot et al., 2013) are consistent with an ice shelf draft above the main thermocline (Figures 1a and 2a–2c).

Combining our new observations with those from earlier cruises allows us to speculate on the interannual variability of CDW at the western GIS. CDW was only present below 650 m in the Siple trough in 2000, making the section distinctly colder than those in 2007, 2016, and 2018 (Figure S1). Extending our time series of the cumulative upwelling anomaly to 1992–2018, we find that 2000 lies within a period of anomalously weak upwelling (Figure 4f). The year 2007 is at the end of a period of increasing upwelling (2004–2006) and 2016 and 2018 after another increase in response to the 2015/2016 El Niño. The CDW layer is around 50 m thicker in 2016/2018 than in 2007 and extends to Dean Island (Figure S2). Our mooring records cover the entire range of variability seen in the CDW sections with the cold period in autumn 2017 as cold as 2000 for GW_7. However, Jacobs et al. (2013) find 2000 to be consistently colder than 2007 for observations that cover the other ice shelf fronts of the GIS, suggesting that the differences between the sections represent interannual rather than short-term variability. The year 2000 was also found to be cold in observations from the eastern Amundsen Sea (Assmann et al., 2013; Dutrieux et al., 2014). In combination, our new and the historical observations from the western Getz provide evidence that interannual changes in upwelling at the shelf break control the presence of CDW at the ice shelf front. However, with only 4 years with significant data coverage we cannot draw any robust conclusions about interannual CDW variability in the region.

Acknowledgments
We thank E. P. Abrahamsen for recovering the late 2015 ice shelf edge from a satellite image and for assistance with mooring deployment. We would also like to thank I. Fer for supplying mooring instrumentation, H. Bryhni, J. Rolandsson, and Ham and the crew of RVIB Araon for help with mooring deployment, recovery, mobilization, and logistics. K. M. Assmann and E. Darelius were financed by the Norwegian Research Council through project 231549 (WARM) and 267660 (TOBACO). Support for T. W. Kim and S. H. Lee was provided by the Korea Polar Research Institute grant KOPRI PE18060. The GW_6 and GW_7 mooring data are available at the Norwegian Marine Data Centre (https://nmdc.no) as UIB4 and UIB1, respectively (Darelius et al., 2018). Metadata for the 2016 and 2018 CTD data can be found on the KOPRI database (https://kpdc.kopri.re.kr, ANA06B:KPDC_CTD_AMUNDSEN_2016,ANA08B:KPDC_CTD_AMUNDSEN_2018), and the data may be obtained on request from KOPRI. CTD data from the 2000 (US010402) and 2007 (US034357) RVIB Nathaniel B. Palmer cruises are available from the World Ocean Data Base at https://www.nodc.noaa.gov/OC5/WOD/pr_wod.html.

References

Arndt, J. E., Schenke, H. W., Jakobsson, M., Nitsche, F., Buys, G., Goleby, B., et al. (2013). The International Bathymetric Chart of the Southern Ocean (IBCSO) Version 1.0—A new bathymetric compilation covering circum-Antarctic waters. *Geophysical Research Letters*, *40*, 3111–3117. https://doi.org/10.1002/grl.50413

Arneborg, L., Wåhlin, A. K., Björk, G., Liljebladh, B., & Orsi, A. H (2012). Persistent inflow of warm water onto the central Amundsen shelf. *Nature Geoscience*, *5*, 876–880. https://doi.org/10.1038/ngeo1644

Assmann, K. M., Jenkins, A., Shoosmith, D., Walker, D. P., Jacobs, S. S., & Nicholls, K. W. (2013). Variability of circumpolar deep water transport onto the Amundsen Sea shelf. *Journal of Geophysical Research: Oceans*, *118*, 6603–6620. https://doi.org/10.1002/2013JC008871

Christie, F. D. W., Bingham, R. G., Gourmelen, N., Steig, E. J., Bisset, R. R., Pritchard, H. D., et al. (2018). Glacier change along West Antarctica's Marie Byrd Land Sector and links to inter-decadal atmosphere-ocean variability. *The Cryosphere*, *12*(7), 2461–2479. https://doi.org/10.5194/tc-12-2461-2018

Darelius, E., Fer, I., Assmann, K., & Kim, T. W. (2018). Physical oceanography from Mooring UiB1 and UiB4 in the Amundsen Sea. https://doi.org/10.21335/NMDC-1721053841

Dee, D. P., Uppala, S. M., Simmons, A. J., Berrisford, P., Poli, P., Kobayashi, S., et al. (2011). The ERA-Interim reanalysis: Configuration and performance of the data assimilation system. *Quarterly Journal of the Royal Meteorological Society*, *137*, 553–597. https://doi.org/10.1002/qj.828

Depoorter, M. A., Bamber, J. L., Griggs, J. A., Lenaerts, J. T. M., Ligtenberg, S. R. M., van den Broeke, M. R., & Moholdt, G. (2013). Calving fluxes and basal melt rates of Antarctic ice shelves. *Nature*, *502*, 89–92. https://doi.org/10.1038/nature12567

Dutrieux, P., De Rydt, J., Jenkins, A., Holland, P. R., Ha, H. K., Lee, S. H., et al. (2014). Strong sensitivity of Pine Island ice-shelf melting to climatic variability. *Science*, *343*, 174–178. https://doi.org/10.1126/science.1244341

Greene, C. A., Blankenship, D. D., Gwyther, D. E., Silvano, A., & van Wijk, E. (2017). Wind causes Totten Ice Shelf melt and acceleration. *Science Advances*, *3*(11), e1701681. https://doi.org/10.1126/sciadv.1701681

IOC, SCOR, & IAPSO (2010). The international thermodynamic equation of seawater-2010: Calculation and use of thermodynamics properties. IOC Manuals and Guides 56, UNESCO, 196 pp. [Available online at http://unesdoc.unesco.org/images/0018/001881/188170e.pdf.]

Jacobs, S., Giulivi, C., Dutrieux, P., Rignot, E., Nitsche, F., & Mouginot, J. (2013). Getz Ice Shelf melting response to changes in ocean forcing. *Journal of Geophysical Research: Oceans*, *118*, 4152–4168. https://doi.org/10.1002/jgrc.20298

Jacobs, S. S., Giulivi, C. F., & Mele, P. (2002). Freshening of the Ross Sea during the late 20th century. *Science*, *297*, 386–389. https://doi.org/10.1126/science.1069574

Jacobs, S., Jenkins, A., Hellmer, H., Giulivi, C., Nitsche, F., Huber, B., & Guerrero, R. (2012). The Amundsen Sea and the Antarctic Ice Sheet. *Oceanography*, *25*(3), 154–163. https://doi.org/10.5670/oceanog.2012.90

Kim, T. W., Ha, H. K., Wåhlin, A. K., Lee, S. H., Kim, C. S., Lee, J. H., & Cho, Y. K. (2017). Is Ekman pumping responsible for the seasonal variation of warm circumpolar deep water in the Amundsen Sea? *Continental Shelf Research*, *132*, 38–48. https://doi.org/10.1016/j.csr.2016.09.005

McDougall, T. J., Jackett, D. R., Millero, F. J., Pawlowicz, R., & Barker, P. M. (2012). A global algorithm for estimating absolute salinity. *Ocean Science*, *8*, 1123–1134.

Nakayama, Y., Timmermann, R., Rodehacke, C. B., Schröder, M., & Hellmer, H. H. (2014). Modeling the spreading of glacial meltwater from the Amundsen and Bellingshausen Seas. *Geophysical Research Letters*, *41*, 7942–7949. https://doi.org/10.1002/2014GL061600

Paolo, F. S., Fricker, H. A., & Padman, L. (2015). Volume loss from Antarctic ice shelves is accelerating. *Science*, *348*, 327–331. https://doi.org/10.1126/science.aaa0940

Paolo, F. S., Padman, L., Fricker, H., Adusumilli, S., Howard, S., & Siegfried, M. R. (2018). Response of Pacific-sector Antarctic ice shelves to the El Niño/Southern Oscillation. *Nature Geoscience*, *11*, 121–126. https://doi.org/10.1038/s41561-017-0033-0

Randall-Goodwin, E., Meredith, M. P., Jenkins, A., Yager, P. L., Sherrell, R. M., Abrahamsen, E. P., et al. (2015). Freshwater distributions and water mass structure in the Amundsen Sea Polynya region, Antarctica. *Elementa: Science of the Anthropocene*, *3*, 65. https://doi.org/10.12952/journal.elementa.000065

Rignot, E., Jacobs, S., Mouginot, J., & Scheuchl, B. (2013). Ice-shelf melting around Antarctica. *Science*, *341*, 266–270. https://doi.org/10.1126/science.1235798

Schaffer, J., Timmermann, R., Arndt, J. E., Kristensen, S. S., Mayer, C., Morlighem, M., & Steinhage, D. (2016). A global, high-resolution data set of ice sheet topography, cavity geometry, and ocean bathymetry. *Earth System Science Data*, *8*(2), 543–557. https://doi.org/10.5194/essd-8-543-2016

Spreen, G., Kaleschke, L., & Heygster, G. (2008). Sea ice remote sensing using AMSR-E 89 GHz channels. *Journal of Geophysical Research*, *113*, C02S03. https://doi.org/10.1029/2005JC003384

Stewart, A. L., & Thompson, A. L. (2015). Eddy-mediated transport of warm Circumpolar Deep Water across the Antarctic shelf break. *Geophysical Research Letters*, *42*, 432–440. https://doi.org/10.1002/2014GL062281

Wåhlin, A. K., Kalen, O., Arneborg, L., Björk, G., Carvajal, G. K., Ha, H. K., et al. (2013). Variability of warm deep water inflow in a submarine trough on the Amundsen Sea shelf. *Journal of Physical Oceanography*, *43*, 2054–2070. https://doi.org/10.1175/JPO-D-12-0157.1

Whitworth, T. III, Orsi, A. H., Kim, S.-J., Nowlin, W. D. Jr., & Locarnini, R. A. (1998). Water masses and mixing near the Antarctic slope front. In S. S. Jacobs & R. F. Weiss (Eds.), *Ocean, ice, and atmosphere: Interactions at the Antarctic continental margin, Antarctic Research Series* (Vol. 75, pp. 1–27). Washington D.C.: American Geophysical Union.